Geophysical Research Letters

RESEARCH LETTER
10.1029/2020GL090408

Quantifying Transition Zone Radiative Effects in Longwave Radiation Parameterizations

Babak Jahani[1], Josep Calbó[1], and Josep-Abel González[1]

[1]Departament de Física, Universitat de Girona, Girona, Spain

Key Points:
- The LW radiation parameterizations RRTMG, FLG, and NGO included in WRF-ARW were used for idealized one-dimensional vertical simulations
- Different approximations to transition zone cause substantial uncertainty in the LW radiative effects at top and bottom of the atmosphere
- Neglecting transition zone conditions at high altitudes contributes to larger uncertainties in the total column energy budget

Supporting Information:
- Supporting Information S1

Correspondence to:
B. Jahani,
babak.jahani@udg.edu

Citation:
Jahani, B., Calbó, J., & González, J.-A. (2020). Quantifying transition zone radiative effects in longwave radiation parameterizations. *Geophysical Research Letters*, *47*, e2020GL090408. https://doi.org/10.1029/2020GL090408

Received 17 AUG 2020
Accepted 5 NOV 2020
Accepted article online 9 NOV 2020

Abstract The change in the state of sky from cloudy to cloudless (or vice versa) comprises an additional phase called "transition zone," in which the characteristics of the particle suspension lay between those corresponding to pure clouds and atmospheric aerosols. This phase, however, is usually considered, in atmospheric monitoring and modeling, as an area containing either aerosol or thin clouds. A sensitivity analysis has been performed to assess the longwave radiative effects resulting from different approximations to the transition zone for three radiation parameterizations included in the Weather Research and Forecasting Model. The parameterizations produce important differences (up to 60 W m^{-2}) between radiative effects of optically thin layers of aerosols and clouds (as surrogates for transition zone suspensions) in the longwave region, both at the top and bottom of the atmosphere. Also, differences are greater if the suspension of particles is located at higher altitudes, but smaller in high humidity conditions.

Plain Language Summary The change in the state of sky from cloudy to cloudless (or vice versa) comprises an additional phase called "transition zone," in which the characteristics of the particle suspension lay between those corresponding to a pure cloud and those of atmospheric aerosols. This phase, however, is usually considered, in atmospheric monitoring and modeling, as an area containing either aerosol or thin clouds. This study quantifies the uncertainties that this binary assumption may introduce to the estimation of longwave radiative effects at the top and bottom of the atmosphere by using the Fu-Liou-Gu (FLG), NewGoddard, and Rapid Radiative Transfer Model for General Circulation Model (RRTMG) radiative parameterizations included in the Weather Research and Forecasting Model. The results show that there are important differences between optically thin clouds and aerosols in longwave region, which may cause substantial uncertainties in the radiative effects at the top and bottom of the atmosphere (up to 60 W m^{-2}) if they are used to approximate transition zone conditions. Results are important due to the role that longwave radiation plays in the radiative balance that drives the Earth's climate.

1. Introduction

Aerosols and clouds, as two particular cases of a single phenomenon (i.e., a suspension of particles in the air), are important components in the climate system. They significantly affect the Earth energy budget by scattering, absorbing, and emitting radiation in the atmosphere. Although aerosols and clouds interact and affect each other's properties, their radiative properties and effects are usually treated separately in climate, meteorological, and weather forecasting studies (Redemann et al., 2009; Spencer et al., 2019; Várnai et al., 2017). Thus, in such studies usually a discrimination between the cloudy and noncloudy sky (which contains a certain aerosol load) is required.

In theory, there are distinct differences between characteristics and origin of fully developed clouds and aerosols, which makes it possible to distinguish them from each other (Liu et al., 2009; Michalsky et al., 2010; Platnick et al., 2003). However, what is categorized as a cloud based on one method may be categorized differently based on another. Additionally, there are some conditions at which regardless of the method utilized, discrimination among them becomes challenging (Calbó et al., 2017; Fuchs & Cermak, 2015; Wollner et al., 2014). Specifically, the change in the state of sky from cloudy to cloudless (or vice versa) occurs gradually, and it comprises an additional phase called "transition zone" (or "twilight zone"). At this phase, the microphysical and radiative characteristics of the suspended particles in the atmosphere are in transition between those corresponding to a pure cloud and those corresponding to pure atmospheric aerosols (Koren et al., 2007, 2009). Based on three ground-based observation systems at two midlatitude sites, Calbó et al. (2017) found that the transition zone produces typically an optical depth of less than 0.32, but

it might be found for optical depth as high as 2.00. The transition zone may correspond to different processes/suspensions: hydration and dehydration of aerosols, cloud fragments sheared off from the adjacent clouds, decaying and incipient clouds, and pockets of high humidity that oscillate near saturation (Koren et al., 2009). It has been found that at any time, a large proportion of sky contains particle suspensions with characteristics of the transition zone (Calbó et al., 2017; Charlson et al., 2007; Koren et al., 2009; Schwarz et al., 2017; Várnai & Marshak, 2011; Wollner et al., 2014). Nevertheless, the vast area that potentially may represent the transition zone is usually neglected and assumed as an area that contains either aerosols or optically thin clouds. In other words, radiative and optical properties corresponding to clear- or cloudy-sky are misleadingly used to characterize such transition zone conditions.

This simplified assumption about the state of the sky rises the following question: "How different the radiative effects will be, if an atmospheric layer containing a suspension of particles corresponding to transition zone is assumed as a cloud or as an aerosol layer?" It was found by Jahani et al. (2019) that under ideal conditions, this assumption may lead to substantial differences in the broadband surface shortwave radiative effects simulated by the radiation parameterizations included in the Advanced Research Weather Research and Forecasting model (WRF-ARW). The uncertainties risen from different approximations (describing a situation corresponding to the transition zone as cloud or as aerosol) in the longwave region, however, remain undescribed to our knowledge. For this reason, the current study aims to quantify these uncertainties by applying a sensitivity analysis, for some of the longwave radiation (*lwrad*) parameterizations included in WRF-ARW.

2. Materials and Methods

2.1. Model Description

WRF-ARW is a widely used mesoscale atmospheric model, developed for both research and operational weather forecasting purposes (Powers et al., 2017). There are seven *lwrad* parameterizations included in this model. These parameterizations are also shared with the Model for Prediction Across Scales (MPAS; Ha et al., 2017), which is intended to replace WRF. Among them, three parameterizations which are capable of dealing with aerosol radiative effects in the longwave band were separated from the model structure and adapted for idealized one-dimensional vertical simulations ("sandbox" approach): Fu-Liou-Gu (FLG_{lw}; Gu et al., 2011), Rapid Radiative Transfer Model for General Circulation Models ($RRTMG_{lw}$; Iacono et al., 2008), and NewGoddard (NGO_{lw}; Chou & Suarez, 1999). These parameterizations were then used to simulate the downwelling longwave irradiance ($E\downarrow$) and the upwelling longwave irradiance ($E\uparrow$) at the model levels, including ground surface ($E_{bot}\downarrow$), and top of the atmosphere, $E_{top}\uparrow$. Throughout this paper, we give positive and negative sign to the physically downwelling and upwelling irradiances, respectively.

In the parameterization FLG_{lw}, the longwave region is divided into 12 spectral bands starting from 4.55 μm. In the case of the parameterizations $RRTMG_{lw}$ and NGO_{lw}, the longwave region starts from 3.33 μm and is divided into 16 and 10 spectral bands, respectively. These *lwrad* parameterizations use different methods for solving the Radiative Transfer Equation (RTE) and obtaining cloud optical properties. These methods are the same as the ones used by their corresponding shortwave schemes, which are described in Chou and Suarez (1999), Iacono et al. (2008), and Gu et al. (2011), respectively. These parameterizations are also different when dealing with the radiative effects of the aerosols and clouds. The parameterizations NGO_{lw} and FLG_{lw} deal with longwave scattering due to atmospheric particles (clouds and aerosols) and calculate their radiative effects based on their extinction coefficient (δ), single scattering albedo (ω), and asymmetry factor (g). In these two parameterizations, the band-averaged values of δ, ω, and g (at each layer) corresponding to aerosols are directly inputed to the RTE solver, whereas the band-averaged cloud optical properties (δ, ω, and g) at each level are calculated based on the input values of droplet/crystal effective radii, liquid/ice water mixing ratio, and temperature, using the cloud parameterizations included in the *lwrad* parameterizations. In $RRTMG_{lw}$, however, cloud and aerosol optical depths (at each spectral band and layer) are the only relevant input to the RTE solver. Indeed, in $RRTMG_{lw}$, the atmosphere is assumed as a nonscattering medium ($\omega = 0$) and the diffusivity angle for all of the atmospheric components is assumed to be the same and is calculated (at each spectral band and layer) as a function of water vapor content.

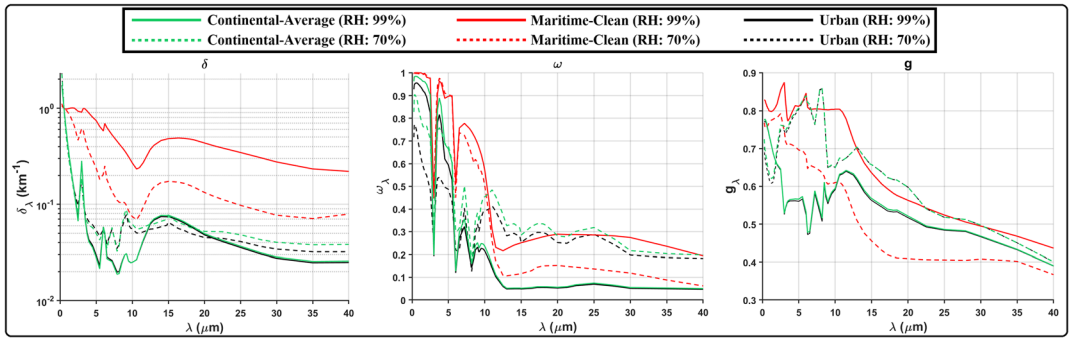

Figure 1. Spectral optical characteristics (extinction coefficient, δ_λ; single scattering albedo, ω_λ; asymmetry factor, g_λ) corresponding to continental-average, maritime-clean, and urban aerosol models at relative humidities equal to 70% and 99% as described in Hess et al. (1998) for $\tau_{0.550} = 1.00$.

2.2. Experiment Setup

The methodology adopted for quantifying the uncertainties risen from different approximations (as cloud or aerosol) to the transition zone in the *lwrad* parameterizations consists of (i) considering cloud- and aerosol-free atmospheres as reference setups, (ii) using the isolated radiation parameterizations to simulate longwave irradiances (upwelling and downwelling) by adding homogeneous layers of cloud—resulting from different combinations of crystal/droplet sizes and liquid/ice water content—or aerosol—with different optical characteristics—to the reference setup, (iii) calculating the radiative effects (RE, W m^{-2}) due to the different cloud/aerosol layers, and (iv) analyzing differences in the simulated REs for both $E_{bot}\downarrow$ (hereafter denoted as $RE_{bot}\downarrow$) and $E_{top}\uparrow$ ($RE_{top}\uparrow$). Here, the term "uncertainty" is defined as the range of REs resulting from describing a situation corresponding to the transition zone as cloud or as aerosol. This methodology is based on the assumption that the radiative effects of the particles with the characteristics of the transition zone are between those corresponding to aerosols and clouds, and thus, the uncertainty calculated this way should be greater than (and hence cover) the difference between the transition zone and pure cloud or aerosol suspensions.

In a cloud- and aerosol-free atmosphere the *lwrad* transfer is dominated by the tropospheric water vapor, due to the spectral extent of its absorbing properties (Clough & Iacono, 1995). Additionally, the amount of *lwrad* emitted by the atmospheric particles/molecules and by the Earth surface is highly affected by temperature. For these reasons, the present study was carried out under both winter and summer conditions. To this aim, the standard midlatitude cloud- and aerosol-free summer and winter atmosphere profiles given in Anderson et al. (1986) were considered as the reference setups. For other atmospheric gases (O_3, CO_2, ...), the precribed profiles included in the parameterizations were used. In all simulations, the model surface and top were set at 0 and 30 km, respectively, and the atmospheric column was divided in 30 layers with equal physical thickness (1 km for each layer). The surface emissivity was fixed to 0.97.

The clouds considered in this study consist of: (i) ice clouds (physical thickness: 1 km, altitude: between 7–8 km) with crystal effective radii (r_e) ranging between 10 and 120 μm and (ii) liquid clouds (physical thickness: 1 km, altitude: between 1 and 2 km) with droplet r_e ranging between 2.5 and 15 μm. The aerosols used consist of six typical aerosol models described in OPAC (Optical Properties of Aerosols and Clouds) aerosol data base (Hess et al., 1998), at different hydration stages (relative humidity: 70–99%): (i) urban; (ii) continental-clean; (iii) continental-average; (vi) continental-polluted; (v) maritime-clean; and (vi) maritime-polluted. The spectral data regarding to aerosol optical properties (extinction coefficient, δ_λ; single scattering albedo, ω_λ; asymmetry factor, g_λ) obtained from OPAC (provided in 61 wavelengths between 0.25 and 40.00 μm) was then transformed to band-averaged values according to the spectral bands of the parameterizations. Figure 1 illustrates the spectral optical characteristics corresponding to the example of continental-average, maritime-clean, and urban aerosol models at relative humidities equal to 70% and 99%. In this figure, δ_λ values correspond to the particle concentrations which produce an optical depth at the 0.550 μm wavelength (τ) equal to 1.00 (assuming a physical thickness of 1 km). This figure shows that the continental-average and urban aerosol models described in Hess et al. (1998) have similar optical

properties, specially at higher hydration levels. This is mainly because both aerosol models are a composition of three aerosol components: insoluble, soot, and water soluble (with only slight different volumetric mixing ratios at the hydrations levels illustrated here) and for both models, the absorption and the scattering cross sections are dominated by the components water soluble and insoluble, respectively. The size distribution of the particles in these two aerosol models are also similar, but different compared to the maritime-clean aerosol model. The aerosols were placed in single layers with altitudes between 7 and 8 km and between 1 and 2 km (physical thickness for the layers at both altitudes: 1 km) for comparison with ice (Comparison I-a) and liquid (Comparison L-a) clouds, respectively.

In all simulations, the τ assigned to either cloud or aerosol layers (here τ only refers to cloud/aerosol and does not account for the other atmospheric components) was considered to vary between 0.01 and 2.00. This range of τ covers low and high values of τ which can potentially represent a transition zone situation (Calbó et al., 2017) and is also consistent with the range considered in Jahani et al. (2019). For the aerosol layers, the variation in τ was addressed through changing total number concentration of the aerosol particles until obtaining the desired τ (at the band that contains the 0.550 μm wavelength). The values of τ at other spectral bands were determined by multiplying the τ at 0.550 μm by the ratio between τ at the desired band and that at 0.550 μm in the original OPAC database. In case of the cloud layers, as each parameterization uses different methods for determination of the cloud optical properties (these methods are different in many ways, including number of bins considered for r_e, size distribution of the droplets/crystals in the cloud, and databases utilized), for each droplet/crystal size, cloud τ was obtained through trial and error: fixing droplet/crystal size and increasing/decreasing water/ice mixing ratio until obtaining the desired τ (at the band that contains the 0.550 μm wavelength) with a maximum error of ±1%.

The radiative effect of each of the mentioned cloud/aerosol layers on any irradiance *irr* (downwelling or upwelling) at any model level, simulated by each parameterization *par*, for a given τ ($RE_{irr,par}(\tau)$) was calculated according to Equation 1:

$$RE_{irr,par}(\tau) = E_{irr,par}(\tau) - E_{irr,par}(0) \quad (1)$$

The irradiance $E_{irr,par}(0)$ corresponds to the simulation for the reference setups (i.e., clean and clear, summer and winter, and atmospheres).

3. Radiative Effects

Vertical profiles of the downwelling ($E\downarrow$, positive values) and upwelling ($E\uparrow$, negative values) longwave irradiances simulated by the parameterizations NGO_{lw}, FLG_{lw}, and $RRTMG_{lw}$ under reference setups are provided in Figure 2. According to Figure 2, both $E_{top}\uparrow$ and $E_{bot}\downarrow$ are much larger (in absolute sense) in summer than in winter, because of higher temperatures and larger water vapor amount in the whole atmosphere. Furthermore, as expected for both summer and winter setups, most changes in $E\uparrow$ and $E\downarrow$ occur in the troposphere (i.e., below 12–15 km). This figure also reveals that the differences among the irradiances simulated by FLG_{lw} and NGO_{lw} are very tiny (<3.8 W m^{-2}), while larger differences are visible with those simulated by $RRTMG_{lw}$. Specifically, $RRTMG_{lw}$ simulates less (absolute) $E\uparrow$ and more $E\downarrow$ compared with FLG_{lw} and NGO_{lw}. The reason for this difference, to a large extent, is the different treatment of diffusivity angle: In $RRTMG_{lw}$ it is computed for all atmospheric components as a function of total column water vapor content (Iacono et al., 2008), whereas in FLG_{lw} and NGO_{lw}, it is determined according their asymmetry factor.

Figure 3 shows the values of $RE_{bot}\downarrow$ and $RE_{top}\uparrow$ resulting from different approximations to the transition zone (describing a situation corresponding to the transition zone as cloud or as aerosol) for τ = 0.01–2.00, based on the three parameterizations. In this figure, the upper panel is dedicated to the comparison between the RE of high (ice) clouds and aerosols (Comparison I-a), and the lower panel to the comparison between the RE of low (liquid) clouds and aerosols (Comparison L-a). In each single plot, the lines of the same type and color mark the maximum and minimum possible values of $RE_{bot}\downarrow$ (blue) and $RE_{top}\uparrow$ (black) due to different cloud (dashed lines) or aerosol (solid lines) approximations. In each single plot, the lower and upper colored areas represent the uncertainty (associated with describing a situation corresponding to the transition zone as cloud or aerosol), which we define here as the range ($\Delta RE_{bot}\downarrow$, blue) of the values of $RE_{bot}\downarrow$ (actually accounting for the uncertainty in $E_{bot}\downarrow$) and the range ($\Delta RE_{top}\uparrow$, pink) of the values of $RE_{top}\uparrow$

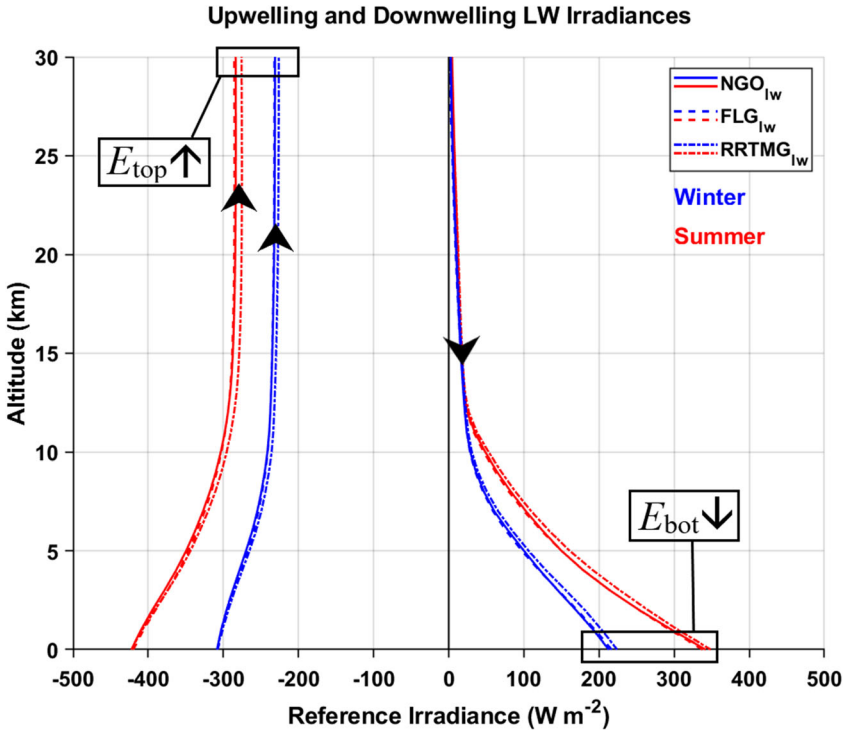

Figure 2. Vertical profiles of the downwelling ($E\downarrow$) and upwelling ($E\uparrow$) *lwrad* simulated by the parameterizations NGO_{lw}, FLG_{lw}, and $RRTMG_{lw}$ for the summer (red lines) and winter (blue lines) reference setups.

(accounting for the uncertainty in $E_{top}\uparrow$). For all parameterizations, adding a cloud/aerosol layer with any τ results in positive $RE_{bot}\downarrow$ and $RE_{top}\uparrow$. In other words, it causes an increase in $E_{bot}\downarrow$ (positive sign, as downwelling) but a reduction in $E_{top}\uparrow$ (negative sign, as upwelling) compared to their corresponding reference irradiances. The increase in $E_{bot}\downarrow$ is due to the downward emission from cloud/aerosol layer, which (despite being far from a blackbody, as the amount of suspended particles is relatively small given the low range of τ considered) is performed at a temperature higher than the brightness temperature of the clear atmosphere. The reduction in the absolute value of $E_{top}\uparrow$ is because the upward emission of the layer is performed at a temperature which is lower than that of the ground, and also due to the fact that cloud/aerosol layer is absorbing some of the $E\uparrow$ emitted by the surface.

In Figure 3 some small differences between the cloud REs simulated by the parameterizations FLG_{lw} and NGO_{lw} are evident. They originate from the difference in the methods used by the parameterizations for solving the RTE, obtaining the cloud optical properties, as well as the number and limits of the spectral bands used. However, despite these differences, the results obtained from FLG_{lw} and NGO_{lw} show that, under all tested conditions, there are distinct and important differences between the REs of aerosols and clouds in the longwave region, which are evident in both $RE_{bot}\downarrow$ and $RE_{top}\uparrow$. This means that assuming a condition corresponding to the transition zone as cloud or aerosol may cause large uncertainties (up to 60.0 W m^{-2} for $\tau = 2.00$, the largest optical depth studied here) in the simulation of $RE_{bot}\downarrow$ and $RE_{top}\uparrow$. This uncertainty seems to be small compared to what was reported in Jahani et al. (2019) for the shortwave radiation. However, it is a rather noticeable value when compared to the $E_{bot}\downarrow$ (217–338 W m^{-2}) and $E_{top}\uparrow$ (232–286 W m^{-2}) for the reference setups (Figure 2), which are the result of the emission and absorption by atmospheric gases. According to Figure 3, even at a relatively low τ of 0.1, $\Delta RE_{bot}\downarrow$ ranges (depending on layer height and season) between 2.2–6.6 and 2.2–7.2 W m^{-2} based on FLG_{lw} and NGO_{lw} simulations, respectively. At the same τ, $\Delta RE_{top}\uparrow$ comprises 1.2–6.5 and 0.5–6.1 W m^{-2} based on FLG_{lw} and NGO_{lw} simulations, respectively. However, it is worth mentioning that results obtained from NGO_{lw} show that there are cases where REs of clouds and aerosols may overlap: liquid clouds with small droplets (r_e: 2.5 μm) and highly hydrated maritime aerosols (relative humidity: 99%; r_e: 2.3–3.0 μm).

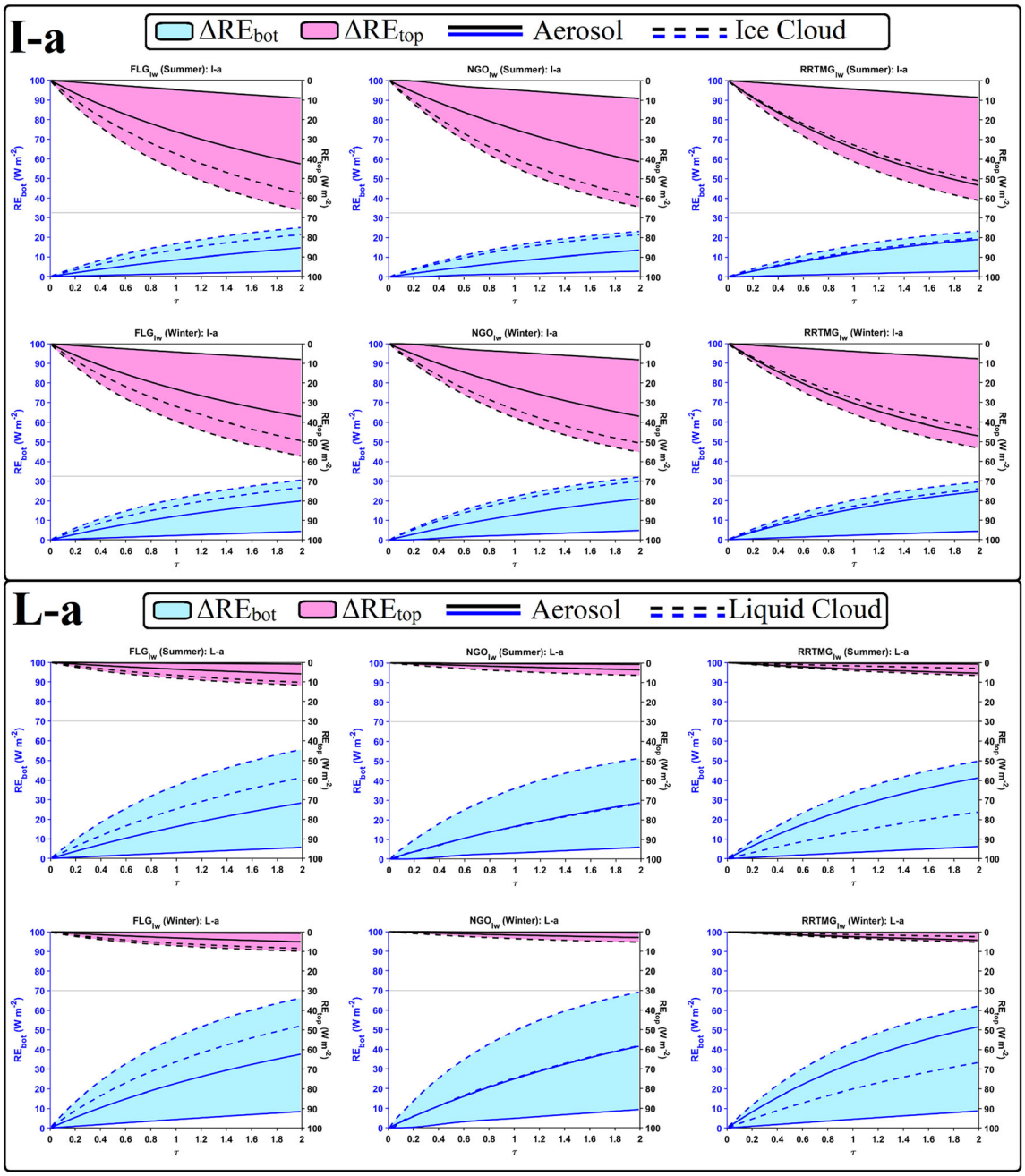

Figure 3. The simulated values of $RE_{bot}\downarrow$ (blue lines, left axis) and $RE_{top}\uparrow$ (black lines, right axis) resulted from different approximations to the transition zone versus $\tau_{0.550}$ (0.01–2.00) for winter and summer atmospheric profiles based on FLG_{lw}, NGO_{lw}, and $RRTMG_{lw}$ simulations (Note: upper panel corresponds to Case "I-a" and the lower panel to "L-a").

The results obtained from $RRTMG_{lw}$, however, are somewhat different from those obtained from FLG_{lw} and NGO_{lw}. According to $RRTMG_{lw}$ simulations, large hydrated aerosols (r_e: 2.3–3.0 μm) produce REs similar to ice/liquid clouds with crystal/droplet r_e as large as 10.0 μm, which results in a smaller range of RE and thus lower uncertainties compared to FLG_{lw} and NGO_{lw} (<45.0 W m^{-2} for $\tau = 2.00$). This is mainly because $RRTMG_{lw}$ deals with *lwrad* in less details compared with FLG_{lw} and NGO_{lw}. Specifically, in this parameterization, longwave scattering due to clouds and aerosols is neglected ($\omega = 0$), and the spectral behavior of the extinction coefficient is considered as the only source of difference among clouds and aerosols of different type. Due to the simplicity of $RRTMG_{lw}$ in dealing with *lwrad* in comparison with the two other

parameterizations, hereafter discussion about transition zone REs will mainly be addressed according to the results obtained from FLG_{lw} and NGO_{lw}.

Figure 3 also shows that for the range of τ studied and in both seasons, the values of $RE_{top}\uparrow$ and $\Delta RE_{top}\uparrow$ simulated under the case I-a are always greater than those of the Case L-a. This is consistent with the results of Mishra et al. (2015) and Mitchell and Finnegan (2009) and means that the higher the layer (where cloud-aerosol confusion happens) is, the greater the uncertainties in the simulation of $E_{top}\uparrow$ are. Thus, as the amount of $E\downarrow$ at the top of the atmosphere is negligible, transition zone conditions at high altitudes will contribute to larger uncertainties in the determination of the longwave radiative forcing and the atmospheric cooling rate. Correspondingly, the $\Delta RE_{bot}\downarrow$ simulated by both parameterizations under the Case L-a is always greater than that of the Case I-a. Detailed information about the vertical behavior of RE at different levels of the atmosphere (in particular at the levels just above and below the cloud/aerosol layers), for the example, of $\tau = 1.00$ is provided in Figure S1 in the supporting information. According to this figure, the values of ΔREs (both upwelling and downwelling) at top and base of the cloud/aerosol layers are indeed greater under Case I-a compared to L-a. The reason for smaller $RE_{bot}\downarrow$ in the Case I-a is that the emitted radiation needs to pass through a (physically and optically) thicker path in the troposphere and thus is subjected to a greater absorption. As a result, the $E\downarrow$ emitted under I-a cases is more strongly attenuated. Furthermore, as Figure S1 shows, for both comparison cases the absorption is even stronger in the layers beneath the cloud/aerosol layers in summer, which is due to larger amount of water vapor in the summer setup (Clough & Iacono, 1995).

4. Conclusions and Discussions

This study has shown that for the range of τ studied (0.01–2.00), there are some differences between parameterizations NGO_{lw} and FLG_{lw} regarding the magnitude of the simulated irradiances, which, however, lead to very similar radiative effect ranges (ΔREs, used as an approximation to uncertainties). $RRTMG_{lw}$, on its side, produces somewhat different irradiances, which result in slightly lower radiative effect ranges. For all parameterizations, when adding a cloud/aerosol layer (with any τ), $E_{top}\uparrow$ decreases (in absolute value), because the upward emission of the layer is performed at a temperature which is lower than that of the ground and $E_{bot}\downarrow$ increases (due to the downward emission from cloud/aerosol layer), resulting in positive $RE_{bot}\downarrow$ and $RE_{top}\uparrow$. The REs simulated by NGO_{lw} and FLG_{lw} show that, under all tested conditions, there are distinct and important differences between the REs of aerosol and clouds in the longwave region, which may result in uncertainties up to ~60W m^{-2} at $\tau = 2.00$. Even at very small τ of 0.10, assuming a situation corresponding to the transition zone as cloud or aerosol may lead to a noticeable amount of $\Delta RE_{top}\uparrow$ (0.5–6.5 W m^{-2}, values depending on layer height and season) and $\Delta RE_{bot}\downarrow$ (2.2–7.2 W m^{-2}). Although this uncertainty has been computed from physical modeling and refers only to local and temporary effects, it deserve to receive attention, because transition zone conditions may affect a vast area of the global atmosphere, therefore a significant proportion of sky at any time is covered with such a particle suspension according with several studies (Calbó et al., 2017; Fuchs & Cermak, 2015; Koren et al., 2007; Schwarz et al., 2017). This amount of uncertainty over a large area may add incertitude to, or explain a part of the doubts associated with, the description of global energy balance and its evolution in combination with the effects of other atmospheric components, such as the well-mixed anthropogenic greenhouse gases (which have produced a global scale radiative forcing of 2.83 ± 0.29 W m^{-2} over 1750–2011; Myhre et al., 2013).

The results also suggest that different approximations to the transition zone for a suspension of particles at higher altitudes has large impacts on the energy budget in the whole column of the atmosphere. In contrast, different approximations to the transition zone at lower altitudes mainly affects the surface energy budget. The results obtained in this study underline the importance of the transition zone in the longwave spectral region and show that different approximations (as cloud or aerosol) to the transition zone may introduce relatively large uncertainties to our understanding about the energy balance in the atmosphere. This is so because a discrimination about the cloudy and cloud-free skies is required in climate studies, but in many of them the area corresponding to the transition zone is either categorized as cloud or aerosol. It should be noted that these uncertainties are not limited to observational studies, because the data obtained from observations are used for running the atmospheric models. This means that even if a certain model is capable of treating clouds and aerosols as continuum fields, the error in the initial input data may introduce large

uncertainties to how energy is transferred in different layers of the model, which, through heating/cooling rates, may significantly affect the model dynamics. Also, a comparison between the simulations of the three parameterizations show that even though the interactions between clouds and aerosols may be well defined in the microphysical schemes of a weather forecasting model, the interactions of the suspensions of particles (clouds and aerosols, more or less hydrated) with radiation may be defined differently in the radiation schemes: in NGO_{lw}, liquid clouds with small droplets (r_e: 2.5 μm) and highly hydrated maritime aerosols (r_e: 2.2.3–3.0 μm) produce very similar REs; whereas, in FLG_{lw}, there is no overlap between the REs of the aerosols and clouds; and in $RRTMG_{lw}$ the REs simulated for large hydrated aerosols (r_e: 2.3–3.0 μm) are similar to those of ice and liquid clouds with crystal/droplet sizes as large as 10.0 μm.

These findings and those obtained by Jahani et al. (2019) for the shortwave region encourage studying the links between these differences in the shortwave and longwave REs and model dynamics. These uncertainties associated with the transition zone REs show the need of defining an additional intermediate phase between the cloudy and clear skies; alternatively, a continuous treatment of such suspensions of particles (from pure, dry aerosols to typical clouds), as well as their coexistence in some situations could also be habilitated in the radiation parameterizations. This may be done through introducing a new set of optical properties for transition zone in models based on the observations, an interpolation between the radiative/optical properties of hydrated aerosols and clouds (some adjusted size distributions laying between those typical of aerosol and those typical for clouds), or including in the parameterizations the aerosol optical properties for relative humidities close to and above saturation. All of these proposals, however, may eventually require defining an index (or a set of indices) to decide about the phase of the particles (aerosol, transition zone, and cloud). Also, studying the radiative behavior of particle suspensions at the transition zone, as well as exploring the size distribution and the composition of particles in the regions around the clouds based on in situ measurements may help researchers to identify such cases. Moreover, it should be noticed that the present study is rather theoretical and limited to (i) two midlatitude atmospheric profiles, (ii) six aerosol types (with characteristics that may be incompatible with their vertical position and relative humidity < 100%), and (iii) homogeneous vertical layers of clouds and aerosols. Thus, the transition zone REs under real conditions (including three-dimensional effects) as well as their effect on the climate system, still need to be further investigated.

Data Availability Statement

The source codes of WRF-ARW model Version 4.0 are freely accessible online (http://www2.mmm.ucar.edu/wrf/users/download/get_source.html). The band-averaged OPAC aerosol optical properties used and the results summarized in Figures 3 and S1 can be downloaded online (http://doi.org/10.5281/zenodo.3987788).

Acknowledgments
This study is funded by the Spanish Ministry of Economy and Competitiveness (project NUBESOL, CGL2014-55976-R), Spanish Ministry of Science and Innovation (project NUBESOL-2, PID2019-105901RB-I00), and University of Girona (project PONTUdG2019/05). Babak Jahani holds a FI-AGAUR PhD grant (2018FI_B_00830) provided by the Government of Catalonia (Universities and Research Secretariat) and the European Union.

References

Anderson, G. P., Clough, S. A., Kneizys, F. X., Chetwynd, J. H., & Shettle, E. P. (1986). AFGL atmospheric constituent profiles (0–120km). *Technical Report*. *AFGL-TR-86–0110*, (954), 46.

Calbó, J., Long, C. N., González, J. A., Augustine, J., & McComiskey, A. (2017). The thin border between cloud and aerosol: Sensitivity of several ground based observation techniques. *Atmospheric Research*, *196*(May), 248–260. https://doi.org/10.1016/j.atmosres.2017.06.010

Charlson, R. J., Ackerman, A. S., Bender, F. A. M., Anderson, T. L., & Liu, Z. (2007). On the climate forcing consequences of the albedo continuum between cloudy and clear air. *Tellus, Series B: Chemical and Physical Meteorology*, *59*(4), 715–727. https://doi.org/10.1111/j.1600-0889.2007.00297.x

Chou, M.-D., & Suarez, M. J. (1999). A solar radiation parameterization (CLIRAD-SW) for atmospheric studies. *NASA Technical Memorandum*, *15*, 44. Retrieved from http://www2.mmm.ucar.edu/wrf/users/phys_refs/SW_LW/Goddard_part1.pdf

Clough, S. A., & Iacono, M. J. (1995). Line-by-line calculation of atmospheric fluxes and cooling rates 2. Application to carbon dioxide, ozone, methane, nitrous oxide and the halocarbons. *Journal of Geophysical Research*, *100*(D8). https://doi.org/10.1029/95JD01386

Fuchs, J., & Cermak, J. (2015). Where aerosols become clouds-potential for global analysis based on CALIPSO data. *Remote Sensing*, *7*(4), 4178–4190. https://doi.org/10.3390/rs70404178

Gu, Y., Liou, K. N., Ou, S. C., & Fovell, R. (2011). Cirrus cloud simulations using WRF with improved radiation parameterization and increased vertical resolution. *Journal of Geophysical Research*, *116*, D06119. https://doi.org/10.1029/2010JD014574

Ha, S., Snyder, C., Skamarock, W. C., Anderson, J., & Collins, N. (2017). Ensemble Kalman filter data assimilation for the Model for Prediction Across Scales (MPAS). *Monthly Weather Review*, *145*(11), 4673–4692. https://doi.org/10.1175/MWR-D-17-0145.1

Hess, M., Koepke, P., & Schult, I. (1998). Optical properties of aerosols and clouds. *Bulletin of the American Meteorological Society*, *79*(5), 831–844. https://doi.org/10.1175/1520-0477(1998)079<0831:OPOAAC>2.0.CO;2

Iacono, M. J., Delamere, J. S., Mlawer, E. J., Shephard, M. W., Clough, S. A., & Collins, W. D. (2008). Radiative forcing by long-lived greenhouse gases: Calculations with the AER radiative transfer models. *Journal of Geophysical Research*, *113*, D13103. https://doi.org/10.1029/2008JD009944

Jahani, B., Calbó, J., & González, J. (2019). Transition zone radiative effects in shortwave radiation parameterizations: Case of weather research and forecasting model. *Journal of Geophysical Research: Atmospheres*, *124*, 13,091–13,104. https://doi.org/10.1029/2019JD031064

Koren, I., Feingold, G., Jiang, H., & Altaratz, O. (2009). Aerosol effects on the inter-cloud region of a small cumulus cloud field. *Geophysical Research Letters*, *36*, 1–5. https://doi.org/10.1029/2009GL037424

Koren, I., Remer, L. A., Kaufman, Y. J., Rudich, Y., & Martins, J. V. (2007). On the twilight zone between clouds and aerosols. *Geophysical Research Letters*, *34*, 1–5. https://doi.org/10.1029/2007GL029253

Liu, Z., Vaughan, M., Winker, D., Kittaka, C., Getzewich, B., Kuehn, R., et al. (2009). The CALIPSO lidar cloud and aerosol discrimination: Version 2 algorithm and initial assessment of performance. *Journal of Atmospheric and Oceanic Technology*, *26*(7), 1198–1213. https://doi.org/10.1175/2009JTECHA1229.1

Michalsky, J., Denn, F., Flynn, C., Hodges, G., Kiedron, P., Koontz, A., et al. (2010). Climatology of aerosol optical depth in north-central Oklahoma: 1992–2008. *Journal of Geophysical Research*, *115*(D7), D07203. https://doi.org/10.1029/2009JD012197

Mishra, A. K., Koren, I., & Rudich, Y. (2015). Effect of aerosol vertical distribution on aerosol-radiation interaction: A theoretical prospect. *Heliyon*, *1*(2), e00036. https://doi.org/10.1016/j.heliyon.2015.e00036

Mitchell, D. L., & Finnegan, W. (2009). Modification of cirrus clouds to reduce global warming. *Environmental Research Letters*, *4*(4). https://doi.org/10.1088/1748-9326/4/4/045102 045102

Myhre, G., Shindell, D., Bréon, F.-M., Collins, W., Fuglestvedt, J., Huang, J., et al. (2013). Anthropogenic and natural radiative forcing. In T. F. Stocker et al. (Eds.), *Climate change 2013: The physical science basis. Contribution of working group I to the fifth assessment report of the Intergovernmental Panel on Climate Change*. Cambridge, UK and New York, NY: Cambridge University Press.

Platnick, S., King, M. D., Ackerman, S. A., Menzel, W. P., Baum, B. A., Riédi, J. C., & Frey, R. A. (2003). The MODIS cloud products: Algorithms and examples from terra. *IEEE Transactions on Geoscience and Remote Sensing*, *41*(2 PART 1), 459–472. https://doi.org/10.1109/TGRS.2002.808301

Powers, J. G., Klemp, J. B., Skamarock, W. C., Davis, C. A., Dudhia, J., Gill, D. O., et al. (2017). The weather research and forecasting model: Overview, system efforts, and future directions. *Bulletin of the American Meteorological Society*, *98*(8), 1717–1737. https://doi.org/10.1175/BAMS-D-15-00308.1

Redemann, J., Zhang, Q., Russell, P. B., Livingston, J. M., & Remer, L. A. (2009). Case studies of aerosol remote sensing in the vicinity of clouds. *Journal of Geophysical Research*, *114*, D06209. https://doi.org/10.1029/2008JD010774

Schwarz, K., Cermak, J., Fuchs, J., & Andersen, H. (2017). Mapping the twilight zone—What we are missing between clouds and aerosols. *Remote Sensing*, *9*(6), 1–10. https://doi.org/10.3390/rs9060577

Spencer, R. S., Levy, R. C., Remer, L. A., Mattoo, S., Arnold, G. T., Hlavka, D. L., et al. (2019). Exploring aerosols near clouds with high-spatial-resolution aircraft remote sensing during SEAC 4 RS. *Journal of Geophysical Research: Atmospheres*, *124*, 2148–2173. https://doi.org/10.1029/2018JD028989

Várnai, T., Marshak, A., & Eck, T. F. (2017). Observation-based study on aerosol optical depth and particle size in partly cloudy regions. *Journal of Geophysical Research: Atmospheres*, *122*, 10,013–10,024. https://doi.org/10.1002/2017JD027028

Várnai, T., & Marshak, A. (2011). Global CALIPSO observations of aerosol changes near clouds. *IEEE Geoscience and Remote Sensing Letters*, *8*(1), 19–23. https://doi.org/10.1109/LGRS.2010.2049982

Wollner, U., Koren, I., Altaratz, O., & Remer, L. A. (2014). On the signature of the cirrus twilight zone. *Environmental Research Letters*, *9*(9). https://doi.org/10.1088/1748-9326/9/9/094010